J. Fluid Mech. (1991), *vol.* 228, *pp.* 343–360
Printed in Great Britain

Entrainment of an eddy at the edge of a jet

By MELVIN E. STERN
Department of Oceanography, Florida State University, Tallahassee, FL 32306, USA

(Received 20 October 1989 and in revised form 27 February 1991)

An inviscid two-dimensional eddy (with maximum circulation $\hat{\Gamma}$ and uniform vorticity $\hat{\zeta}_2 > 0$), surrounded by irrotational fluid is initially located near the edge of a jet, on the other side of which the vorticity $\hat{\zeta}_1 (< \hat{\zeta}_2)$ increases. The interaction causes the eddy to move towards the edge and into the shear flow. Eventually the eddy and the ambient (irrotational) fluid are surrounded by the jet fluid. An average entrainment velocity is computed for a variety of relevant conditions, and found to scale mainly with $(\hat{\Gamma}\hat{\zeta}_1)^{\frac{1}{2}}$. The approximate proportionality constant is somewhat larger than the measured value for three-dimensional (turbulent) jets, suggesting that the two-dimensional mechanism may be qualitatively relevant. The results may also be generalized to study the role of mesoscale eddies in the lateral entrainment of ambient fluid into oceanic jets.

1. Introduction

Entrainment occurs in many different ways and on many different scales in the laboratory, ocean, and atmosphere. The low-Reynolds-number jet issuing from a small nozzle into a fluid of the same density is one example. In this case the molecular viscous forces increase the velocity and vorticity of the ambient fluid, thereby incorporating it in an enhanced downstream transport. This requires a transverse inflow of irrotational fluid into the jet, thereby forcing a larger scale 'recirculation' gyre (extending to the boundary walls of the system).

At very large Reynolds number the entrainment mechanism is intimately connected with the evolution of the large-scale eddies generated by the jet. The sequence of events leading up to turbulent entrainment can be seen in Rockwell & Niccolls' (1972) photographs of hydrogen bubbles in a planar jet. At a small distance downstream from the nozzle, amplifying Kelvin–Helmholtz waves appear in the thin shear layer separating the thicker irrotational jet core from the ambient irrotational fluid, in agreement with the results of a piecewise-uniform vorticity model (Pozrikidis & Higdon 1985), and also with finite-Reynolds-number numerical calculations (Corcos 1981). These also show the subsequent merging of the adjacent vortex cores, which is the next stage in the transition to turbulence, in either the jet problem or the free-shear-layer problem (Roshko 1981; Hussain 1981).

Although the Kelvin–Helmholtz instability and core merger process leads to the 'engulfment' of irrotational fluid in the modified mean vorticity layer, none of that fluid is transported across the actual boundaries of the vortical domains (i.e. the cores). The mixing of such large-scale structures with different vorticities occurs further downstream in the jet, after the onset of a three-dimensional instability of the vortex cores. At this stage mean vorticity exists throughout the jet, and mature large-scale eddies may be generated (on one side of the jet, or the other) by vortex stretching, local instability, and mergers. During its short lifetime this mature

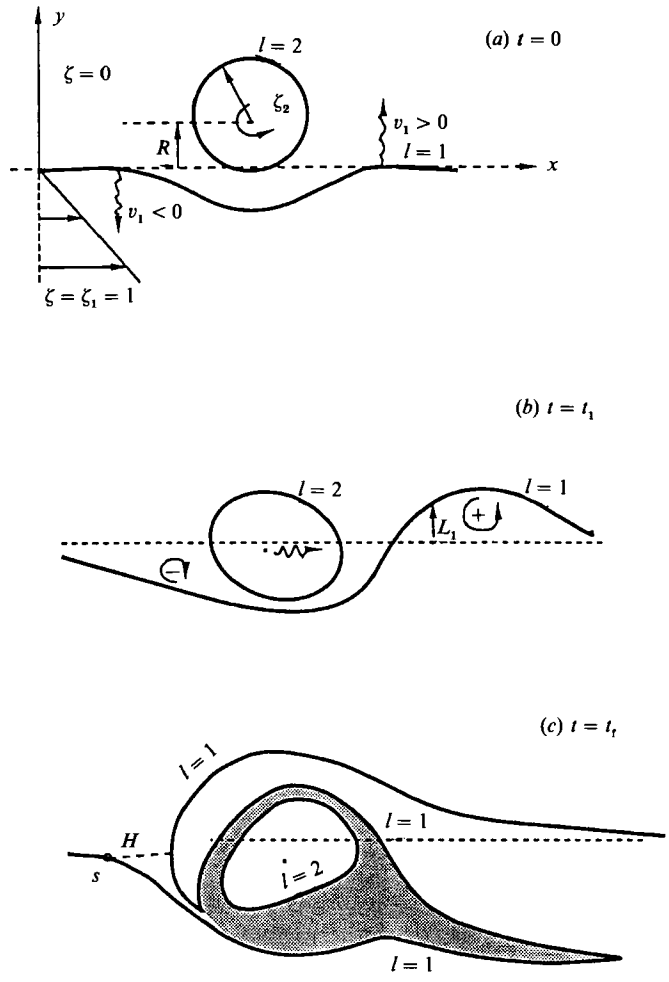

FIGURE 1. Schematic diagram. (*a*) The assumed initial ($t = 0$) state at the outer edge ($l = 1$) of a two-dimensional shear layer, in which the non-dimensional vorticity is $\zeta_1 = 1$. Immediately above ($y > L_1(x,t)$) this interface there is a semi-infinite irrotational layer, and embedded in this is an eddy having non-dimensional area $\pi\rho^2$ and vorticity $\zeta_2 > \zeta_1$. This eddy induces an upward (downward) velocity v_1 on $l = 1$ at x greater (less) than zero. (*b*) The change in L_1 gives rise to $\pm$'vorticity anomalies' in the area between $y = L_1$ and $y = 0$, and the velocity induced by these anomalies causes the centroid of the eddy ($l = 2$) to move downwards into the shear layer. The $x = 0$ origin of the coordinate system moves with the x-velocity of the centroid in all figures. (*c*) At $t_f > t_1$ the eddy and surrounding irrotational fluid are entrained in the jet. H is the shortest distance between the point s and the $l = 1$ branch that has wound counterclockwise around the eddy (see text).

eddy is advected downstream, where it interacts with the somewhat smaller vorticity of the local jet.

Starting at this point we propose to compute the subsequent eddy–shear flow interaction using a highly simplified inviscid, two-dimensional, and piecewise-uniform vorticity model. We will assume a uniform vorticity ζ_1 underneath the upper edge (designated $l = 1$) of our jet (figure 1*a*), and above $l = 1$ there is a semi-infinite irrotational region. Embedded in this is an eddy (whose perimeter is designated by

$l = 2$) of area $\pi\hat{\rho}^2$, vorticity $\hat{\zeta}_2 > \hat{\zeta}_1 > 0$, and circulation $\hat{\Gamma} = \pi\hat{\rho}^2\hat{\zeta}_2$. The centroid of the eddy is initially at a distance $\bar{y}(0) = \hat{R}$ above the undisturbed interface ($y = 0$) of the jet, whose axis (of symmetry) is at $y = -\hat{D}$. The $\hat{D} = \infty$ case considered first corresponds to an eddy interacting mainly with the near edge of the jet, and one aspect of the finite-$\hat{D}$ case is considered subsequently. We shall use $\hat{\zeta}_1^{-1}$ as the time unit and $\hat{\lambda} = (\hat{\Gamma}/\hat{\zeta}_1)^{\frac{1}{2}}$ as the length unit in the subsequent non-dimensionalization, so that the corresponding vorticity of the shear layer (figure 1*a*) is $\zeta_1 = 1$, and $\zeta_2 > 1$ is the non-dimensional eddy vorticity. Then the eddy has non-dimensional area $\pi\rho^2$, circulation $\pi\rho^2\zeta_2 = \hat{\Gamma}/\hat{\lambda}^2\hat{\zeta}_1 = 1$, and $\bar{y}(0) = R$. The interfacial height of l_1 is $y = L_1(x, t)$, and $y = L_2(x, t)$ denote the ordinate of l_2. If the eddy vorticity exceeds that of the shear flow, and if R is small, then we will show that $\bar{y}(t)$ decreases as the upward velocities (figure 1(*b*) induced on the downstream side of $l = 1$ by the eddy cause a wedge of ζ_1 fluid to wrap counterclockwise around the eddy. The decisive stage (figure 1*c*) for entrainment occurs when the downstream branch of the $l = 1$ interface comes into close contact with the upstream branch, thereby irreversibly surrounding both the eddy and the adjacent irrotational fluid inside a 'new' interface.

From the total amount of fluid incorporated into the shear flow, and from the elapsed time, an entrainment velocity $\hat{V}_*$ is defined and computed (§4) for various values of the parameters. The approximately constant value of $\hat{V}_*/(\hat{\Gamma}\hat{\zeta}_1)^{\frac{1}{2}}$ implies that the entrainment velocity depends more on the eddy circulation than on the eddy vorticity (as long as this exceeds $\hat{\zeta}_1$). This is significant in attempting (§7) to relate the mechanism to entrainment in a turbulent jet because the maximum circulation of an eddy is a more appropriate measure of its strength than any single value of the vorticity in the three-dimensional structure.

Brief mention may also be made of another variety of large-Reynolds-number entrainment, one which is essentially two-dimensional insofar as potential vorticity is conserved. The mass (and energy) flux in a quasi-permanent oceanic jet like the Gulf Stream increases downstream from the Straits of Florida (Richardson 1985). The entrainment is accompanied by large and weak recirculating gyres, embedded in which are small-scale and strong mesoscale eddies (these are probably not generated locally). The following barotropic results suggest that the interaction of these eddies with the jet may assist the merging of the gyre water by overcoming any potential vorticity barriers existing at the jet's edge. For further discussion of eddy–shear flow interaction in the ocean see Ikeda & Lygre (1989) and Smith & Bird (1989).

2. Formulation

The following calculations are based on the method of contour dynamics, Zabusky, Hughes & Rogers (1979). Two well-known problems are implicit in figure 1(*a*), one of which, obtained by removing the eddy (i.e. $\hat{\zeta}_2 = 0$) (Stern 1985; Dritschel 1988), concerns the free evolution of a finite-amplitude trough ($l = 1$) on the interface of a shear layer. If the initial amplitude of the trough is large the downstream phase propagation will be followed by nonlinear steepening and 'wavebreaking' of the forward face of the trough. Then $L_1(x, t)$ becomes multi-valued, and as the straining effect of the shear flow continues a long thin $l = 1$ filament extends downstream. The irrotational fluid drawn into the trough in the wavebreaking phase is eventually squeezed back into the $\zeta = 0$ domain, so that very little of the latter is entrained Pullin 1981). We shall show that when a strong eddy ($\zeta_2 > \zeta_1$) is present the situation is entirely different.

The second familiar problem (Melander, Overman & Zabusky 1986) is obtained by

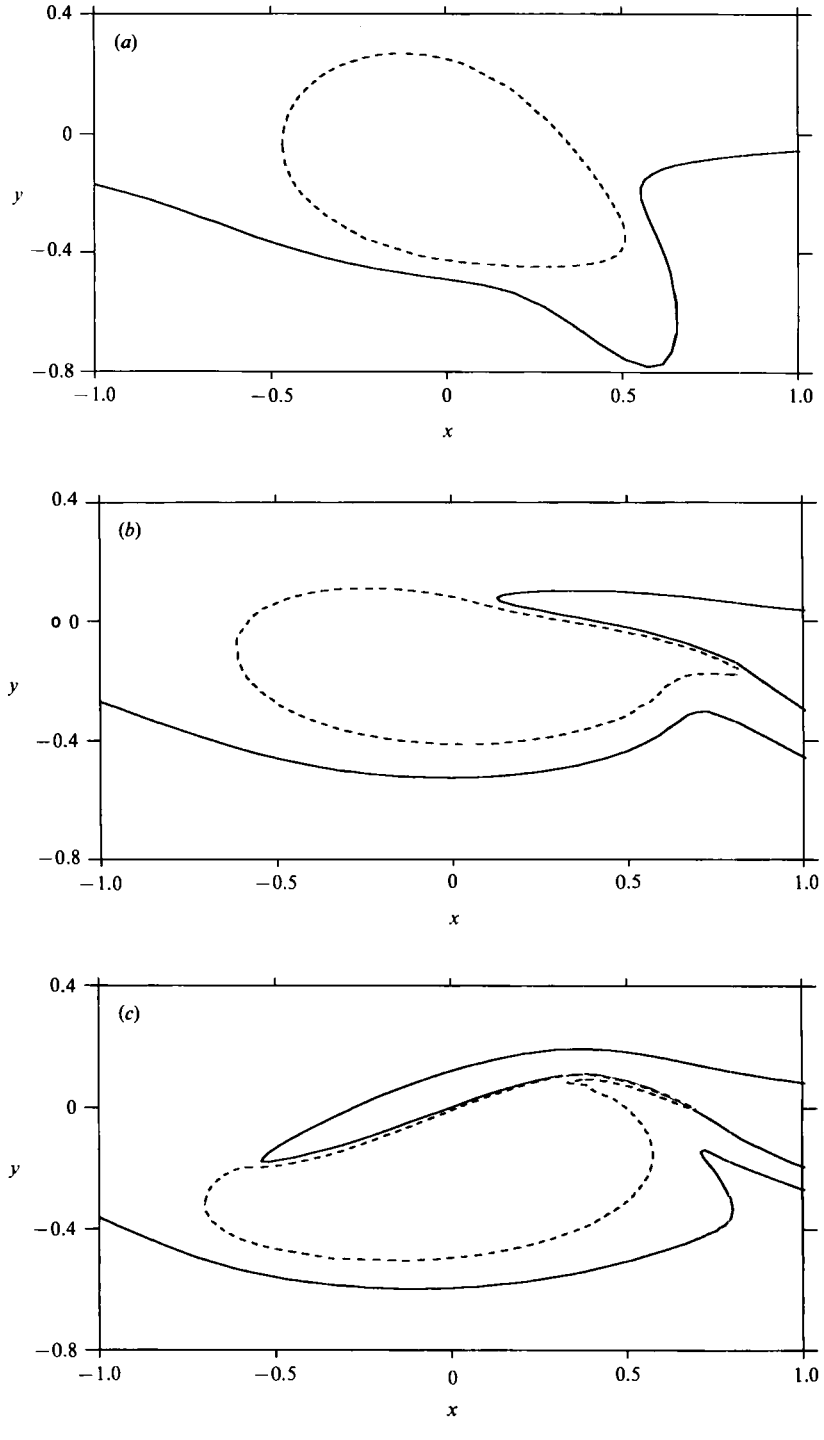

FIGURE 2 (*a–c*). For caption see facing page.

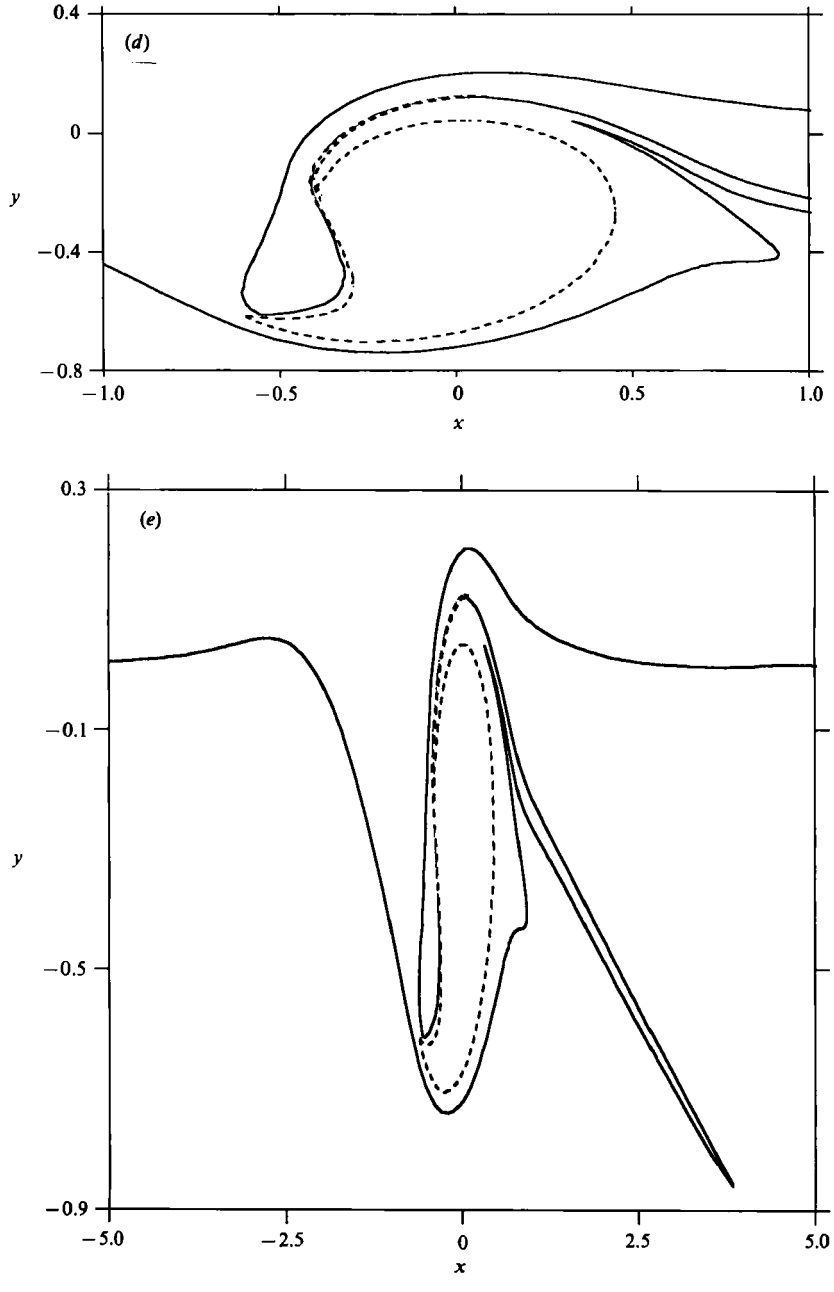

FIGURE 2. The evolution of the interfaces for $\zeta_2 = 2, R = -0.11, \rho = 0.40 = B$. The endpoints of the numerical calculation extend beyond $x = \pm 5.65$. To aid identification here and elsewhere the $l = 2$ curve has been dashed. (*a*) $t = 1$, (*b*) $t = 3$. Note the closing 'gap' between $l = 1$ and the right-hand side of $l = 2$. (*c*) $t = 5$. Note the wedge of $\zeta = 1$ fluid winding around the top of the eddy. (*d*) $t = 7$. Entrainment is virtually complete as the wedge of $\zeta = 1$ fluid approaches the upstream branch ($l = 1$) of the same fluid. (*e*) A large-scale view at $t = 7$. There are 395 points on $l = 1$ and 185 points on $l = 2$. A thin filament emerging from the upper left-hand side of $l = 2$ is nearly coincident with a segment of $l = 1$.

removing the shear layer (i.e. set $\hat{\zeta}_1 = 0$ in figure 1*a*) and by considering the evolution of an (irregular) round eddy ($l = 2$). The algorithm used by Stern (1985) in a variant of this problem is merged with the one used for the $\hat{\zeta}_2 = 0$ problem, in the present study. A preliminary version of the eddy–shear flow interaction using a point vortex was given by Stern & Flierl (1987), but that study was not directed towards the entrainment problem, and no rates were computed.

The well-known piecewise-uniform vorticity model (summarized below for convenience) allows us to express the (x, y)-components of velocity (u, v) as contour integrals on the $l = 1, 2$ boundaries. The contribution of all the vortex elements inside $l = 2$ is given by (2.1)–(2.2), and (2.3)–(2.4*a*, *b*) give the contribution due to $l = 1$. Equation (2.4*b*) gives the velocity associated with the undisturbed interface, while (2.3), (2.4*a*) give the velocities associated with the vortex anomalies lying between $L_1(x, t)$ and the $y = 0$ axis. As indicated by $\pm$ (in figure 1*b*) these anomalies have strength $+1$ where $L_1 > y > 0$, strength -1 where $0 > y > L_1$, and they are responsible for all of the y-component of velocity produced by the disturbed shear flow. These equations are

$$v_2(x, y, t) = \frac{\zeta_2}{4\pi} \oint \mathrm{d}L_2(\xi, t) \ln [(x-\xi)^2 + (y - L_2(\xi, t))^2], \tag{2.1}$$

$$u_2(x, y, t) = \frac{\zeta_2}{4\pi} \oint \mathrm{d}\zeta_2 \ln [(x-\xi)^2 + (y - L_2(\xi, t))^2], \tag{2.2}$$

$$v_1 = \frac{1}{4\pi} \int \mathrm{d}L_1(\xi, t) \ln [(x-\xi)^2 + (y - L_1(\xi, t))^2], \tag{2.3}$$

$$u_1 = \frac{1}{4\pi} \int_{-\infty}^{+\infty} \mathrm{d}\xi \ln \frac{(x-\xi)^2 + (y - L_1(\xi, t))^2}{(x-\xi)^2 + y^2} + \bar{u}(y), \tag{2.4a}$$

$$\bar{u}(y) = \begin{cases} 0 & \text{if} \quad y \geqslant 0 \\ -y & \text{if} \quad y \leqslant 0 \end{cases}, \tag{2.4b}$$

where the contour integrals are taken clockwise for $l = 2$, and from $\xi = -\infty$ to $\xi = +\infty$ in (2.3). The Lagrangian integro-differential equations for a point $[x_l(t), L_l(x_l, t)]$ on interface $l = 1, 2$ are then given by

$$\mathrm{d}L_l/\mathrm{d}t = v_1(x_l, L_l, t) + v_2(x_l, L_l, t) \equiv v(x_l, L_l, t), \tag{2.5}$$

$$\mathrm{d}x_l/\mathrm{d}t = u_1(x_l, L_l, t) + u_2(x_l, L_l, t) = u(x_l, L_l, t). \tag{2.6}$$

The (Lagrangian) boundary conditions on $l = 1$ are $\mathrm{d}L_1/\mathrm{d}t = 0$ and $\mathrm{d}x/\mathrm{d}t = 0$ at $x_1 = \pm\infty$.

The numerical solution was obtained in terms of $N_1(t) \times N_2(t)$ Lagrangian points distributed in a truncated x-interval centred around the centroid of the translating eddy, with endpoints or interior points added or deleted as necessary. The integrals (taken along the contours) are approximated by the trapezoidal rule, with an indentation at the logarithmic singularity, whose contribution is included by means of an analytical approximation. The velocities are then used to advance (x_l, L_l) one time step using a second-order Runge–Kutta approximation. The long-time errors were monitored by recording the area S_2 bounded by $l = 2$, and the integrated L_1, denoted by S_1.

When $D = \infty$ the 'far-field' ($|x_1| \to \infty$) velocities are sensitive to the sum of the eddy circulation and the integrated vorticity anomaly. If this sum vanishes the

t	$\bar{y}$	$\bar{x}$	S_1	S_2
0	−0.11	0	−0.96	0.50
0.5	−0.11	0.12	−0.96	0.50
1.0	−0.11	0.23	−0.96	0.50
2.0	−0.12	0.45	−0.95	0.50
3.0	−0.16	0.68	−0.95	0.50
4.0	−0.20	0.93	−0.95	0.50
5.0	−0.24	1.22	−0.96	0.50
6.0	−0.28	1.54	−0.97	0.50
7.0	−0.32	1.88	−0.98	0.50

TABLE 1. The centroid $(\bar{x}, \bar{y})$ of the eddy, and the areas bounded by $l = 1, 2$. $\zeta_2 = 2$, $R = -0.11$, $\rho = 0.40$, $Q = -0.79$, $B = 0.40$. See figure 2.

velocities decay 'rapidly' (x^{-2}), as is desirable for the truncated calculation, and therefore the initial condition used for the semi-infinite shear layer was taken as

$$\int_{-\infty}^{+\infty} \mathrm{d}x\, L_1(x, 0) = -1. \tag{2.7}$$

This is satisfied by

$$L_1(x, 0) = \frac{Q}{1 + (x/B)^2}, \quad B \equiv -\frac{1}{\pi Q}, \tag{2.8}$$

which is a reasonable representation of the disturbed jet edge when it first encounters a mature eddy. It is equally desirable to have the same kind of balance (yielding small far-field velocities) at all t, and this was realized for the strong interactions which occur when R is small. For the finite-D model (§5), the far-field velocities are always small to order x^{-2}. But in the weak interactions for $D = \infty$ the initial balance (2.7) could not be maintained in the truncated x-interval (for reasons discussed in the Appendix).

The troublesome endpoint and truncation issues in the isolated eddy model are usually eliminated by employing a spatially periodic model, and the results of two such calculations will be mentioned for the sake of comparison. But the 'timewise' evolution of a periodic model is unsatisfactory in many physical problems (like entrainment) where the actual evolution is 'spacewise' (so called). Furthermore, the isolated eddy is a better representation of a large-Reynolds-number entraining event since velocity realizations exhibit small spatial coherence.

3. The round eddy interacting with an unbounded ($D = \infty$) shear layer

Because of (2.7) it is easy to see from figure 1 (*a*) that if R is sufficiently small, then the positive vortices inside $l = 2$, rather than the negative vorticity anomalies above $l = 1$, will determine the sign of the initial v (as indicated by the vertical wiggly arrows) on $l = 1$. This was confirmed by the computed initial velocities for $\zeta_2 = 2$, $R = -0.11$ (figure 2). The centroid of $l = 2$ (figure 1) moves downstream owing to the horizontal velocities induced by the negative vorticity anomalies above $l = 1$, and the origin ($x = 0$) of our coordinate system in all that follows is constrained to move with the centroid.

These initial values of v tend to produce smaller L_1 upstream of the eddy than downstream (figure 1*b*), thereby leading to an asymmetrical distribution of vorticity anomalies, with more negative ones upstream of the centroid and more positive ones downstream. On the other hand, the (free-wave) tendency for the $l = 1$ trough to

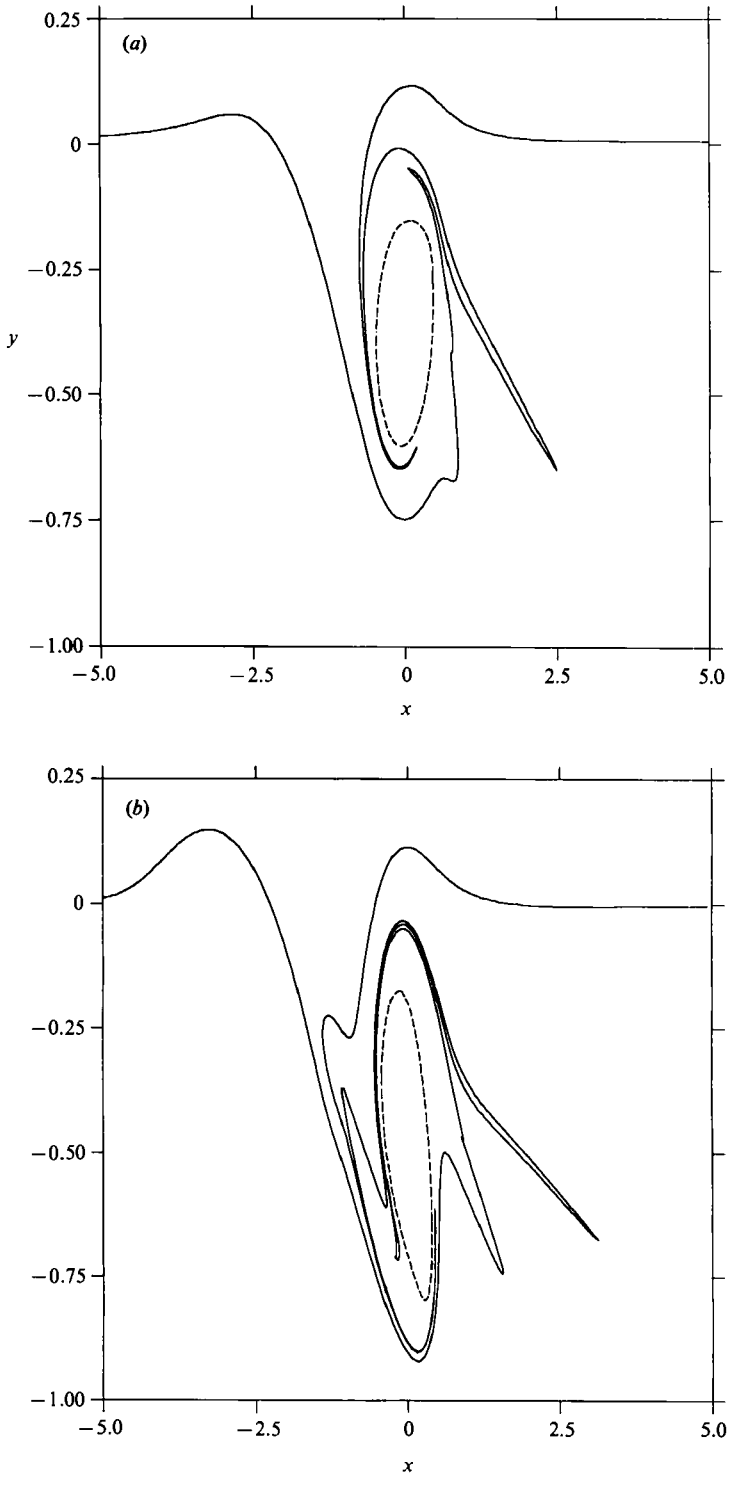

FIGURE 3. The $\zeta_3 = 3$ run. $R = -0.092$, $\rho = 0.32$, $B = 0.49$. (*a*) $t = 7$, (*b*) $t = 10$. The horizontally compressed scale shows the extent of the filamentation, and also the well-behaved interface near the endpoints.

propagate downstream leads to a transfer of negative $l = 1$ anomalies from the upstream side of $l = 2$ to the downstream side. If the latter tendency dominated then the associated vortex anomalies would induce an upward velocity of the centroid, whereas a downward velocity would occur for the former tendency. Both of these effects can be seen in figure 2(*a*), and for small t they tend to cancel, as shown by the constancy of $\bar{y}(t)$ in table 1. But later on (figure 2*b*) we see that the advective and straining effect of the shear flow carries negative vortex anomalies away from the downstream side of the eddy, and figure 2(*b*) clearly shows the dominance of the negative vorticity anomalies on the upstream side of the strong eddy. These cause the centroid to move downward, as confirmed by table 1.

As the eddy descends into the shear layer the $\bar{u}(y)$ term (2.4*b*) causes the downstream speed ($\mathrm{d}\bar{x}/\mathrm{d}t$) of the centroid to increase, and the same is true for the descending particles at the same y on the upstream side of $l = 1$. But the speed decreases for the ascending particles at the same y on the downstream side of $l = 1$. These differential velocities cause the width of the gap between $l = 2$ and $l = 1$ to be smaller on the downstream side than on the upstream side (figure 2*b*). Consequently, the eddy circulation is able to force more irrotational fluid downwards through the larger gap than it can force upwards through the smaller gap, so that irrotational fluid accumulates and is trapped under the descending eddy.

It is easy to understand the anticlockwise winding (figure 2*c*) of a wedge of $\zeta = 1$ fluid. This would also occur (as a passive kinematical effect) even if $\hat{\zeta}_1 = 0$, but for finite $\hat{\zeta}_1$ the positive vorticity anomaly of the wedge (in addition to that of the negative vorticity anomaly) has a crucial dynamical effect in causing the eddy to descend.

Figures 2(*d*) and 2(*e*) show the entrainment phase, in which this wedge or downstream branch of $l = 1$ makes close contact with the upstream branch of $l = 1$, thereby surrounding both the eddy and a mass of ambient ($\zeta = 0$) fluid by shear-flow fluid ($\zeta = 1$). At this stage an essentially multi-connected $l = 1$ curve is produced, even though mathematically complete contact of the branches cannot occur. To all intents and purposes there is a net transport of mass across a ('new') edge of the shear layer formed by 'cutting' the interface at the contact point. From an ensemble of such events a time-average transverse ('entrainment') velocity at the edge of a jet, or at its boundary with the irrotational region, will be computed.

Qualitatively similar results (figure 3 and table 2) are obtained when ζ_2 is multiplied by $\frac{3}{2}$ when ρ is multiplied by $(\frac{2}{3})^{\frac{1}{2}}$, when B is multiplied by $(\frac{3}{2})^{\frac{1}{2}}$, and when the x-interval of integration is increased to reduce endpoint errors caused by this stronger eddy.

In both of these runs R has a small negative value, but by reducing ζ_2 (figure 4) we must increase the radius ρ, and this requires an increased R to avoid contour intersections at $t = 0$. The velocities induced on $l = 1$ are therefore decreased, and this leads to a much longer time for complete entrainment. But in this interval more irrotational fluid can be subducted, and we shall show (§4) that the entrainment velocity is not reduced much. Two of the thinnest filaments in figure 4 ($t = 18$) have reappeared even though their (similar) precursors (at $t = 14$) had been removed by 'contour surgery' to prevent tangling of nearly coincident branches. This surgery was done by inspection, after ascertaining that the area and circulation of the deleted filament was three orders of magnitude smaller than the eddy. Tables 1 and 2 for the strong interaction case show that S_1 and S_2 are approximately conserved (so that mass is conserved in the truncated interval), but table 3 shows that S_1 changes by 20% in this 'weak' interaction case (relatively large R and small ζ_2). This change in

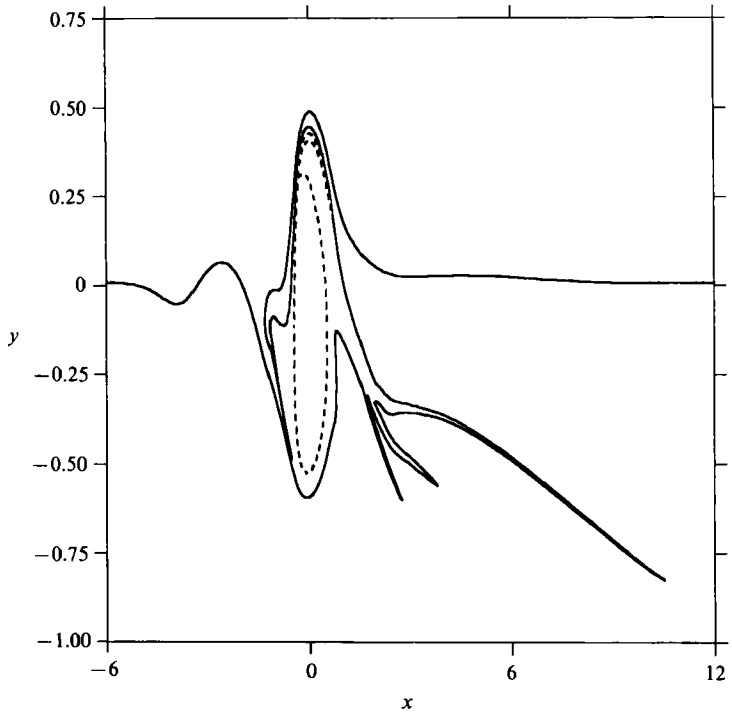

FIGURE 4. The $\zeta_2 = 1.5$ run. $R = 0.098$, $\rho = 0.46$, $B = 0.46$. $t = 18$. The round eddy (dashed curve) has a thin filament emerging from the upper left-hand corner.

t	$\bar{y}$	$\bar{x}$	S_1	S_2
0	−0.09	0	−0.97	0.33
1	−0.10	0.21	−0.97	0.33
2	−0.12	0.42	−0.96	0.33
4	−0.21	0.91	−0.95	0.33
5	−0.27	1.21	−0.95	0.33
6	−0.32	1.56	−0.96	0.33
7	−0.37	1.94	−0.96	0.33
8	−0.41	2.36	−0.98	0.33
9	−0.45	2.82	−1.00	0.33
10	0.47	3.25	−1.00	0.33

TABLE 2. $\zeta_2 = 3$, $R = -0.092$, $\rho = 0.32$, $Q = -0.65$, $B = 0.49$. See figure 3.

S_1 is due to a cumulative endpoint v error, as discussed in the Appendix. To confirm this $\zeta_2 = 1.5$ calculation, we repeated it (not shown) using a periodic (x-wavelength = 12) domain of eddies, employing the well-known (e.g. Pozrikidis & Higdon 1985 periodic Green's function. S_1 was then conserved ($\pm 1.5\%$), and otherwise there were insignificant differences (2%) compared to the computed quantities listed (table 4, row 2) for the isolated eddy.

For an even weaker interaction (table 4, first row) with $\zeta_2 = 1$ the isolated eddy was not entrained, but it merely 'tears' a very thin filament away from the shear layer. The $\zeta_2 = 1$ calculation was also repeated in a periodic domain using a slightly different initial condition ($Q = 0$), but retaining the same minimum initial separation between $l = 1$ and $l = 2$. The initial value of $\bar{y}(0) = 0.77$ decreased to a minimum

t	$\bar{y}$	$\bar{x}$	S_1	S_2
0	0.10	0	−0.98	0.67
2	0.11	0.34	−0.98	0.67
4	0.10	0.65	−0.96	0.67
6	0.06	0.97	−0.94	0.67
8	0.02	1.35	−0.91	0.67
10	−0.02	1.77	−0.88	0.67
12	−0.05	2.22	−0.85	0.67
14	−0.07	2.67	−0.81	0.67
16	−0.08	3.14	−0.81	0.67
18	−0.10	3.64	−0.78	0.67
20	−0.14	4.16	−0.79	0.67

TABLE 3. $\zeta_2 = 1.5$, $R = 0.098$, $\rho = 0.46$, $Q = -0.69$, $B = 0.46$. See figure 4. The non-constancy of S_1 is discussed in the Appendix.

R	$R-Q$	D	t	$\alpha(t)$	$\hat{V}_*/(\hat{\Gamma}\hat{\zeta}_1)^{\frac{1}{2}}$	$\bar{y}(t)$	Remarks
0.41	0.97	∞	22	0	0	0.32	$\zeta_2 = 1$
0.098	0.79	∞	18	1.63	0.091	−0.10	$\zeta_2 = 1.5$
−0.11	0.68	∞	7	0.89	0.13	−0.32	$\zeta_2 = 2$
−0.092	0.56	∞	10	1.00	0.10	−0.47	$\zeta_2 = 3$
−0.11	0.68	∞	8	0.89	0.11	−0.42	$\zeta_2 = \infty$
−0.16	0.97	∞	9	0.90	0.10	−0.56	$\zeta_2 = \infty$
−0.082	0.49	∞	9	0.89	0.098	−0.41	$\zeta_2 = \infty$
−0.11	0.68	1.13	9	0.90	0.10	−0.38	$\zeta_2 = \infty$
−0.11	0.68	0.85	9	0.88	0.097	−0.34	$\zeta_2 = \infty$
0.28	0.28	0.85	9	0.89	0.098	−0.25	$L_1(x,0) = 0$, $\zeta_2 = \infty$
0.28	0.28	0.60	9	0.87	0.095	−0.13	$L_1(x,0) = 0$, $\zeta_2 = \infty$
0.56	0.56	0.85	24	2.17	0.090	0.073	$L_1(x,0) = 0$, $\zeta_2 = \infty$
0.12	0.68	0.85	21	1.44	0.070	−0.079	$\zeta_2 = \infty$

TABLE 4. Summary of entrainment results for a round eddy (finite ζ_2) and for a point vortex ($\zeta_2 = \infty$). $\alpha(t)$ is the total entrained area at time t (non-dimensional units) and $\hat{V}_*$ is the entrainment velocity (dimensional units). The second column is the initial distance of the centre of the vortex from the underlying interface.

$\bar{y}(18) = 0.49$, and then increased, thereby verifying that the $\zeta_2 = 1$ eddy is clearly not entrained. The main effect of such a weak eddy is to force a finite $L_1(x,t)$, which then evolves like a free wave, with wavebreaking and the formation of a very thin filament of irrotational fluid.

In the other limiting case, $\zeta_2/\zeta_1 = \infty$ (equivalent to $\hat{\zeta}_1 \to 0$), the centroid will also not move since the dynamically passive $l = 1$ interface is merely wound around the eddy. If anything, the interface is 'entrained' by the eddy, and not the other way.

4. Computing the rate of entrainment

Entrainment rates cannot be measured 'instantaneously' but require time (or ensemble) averages over events originating when strong eddies come in close contact with the jet's edge, and ending when the eddy becomes (almost) completely surrounded. The quantification of this is as follows.

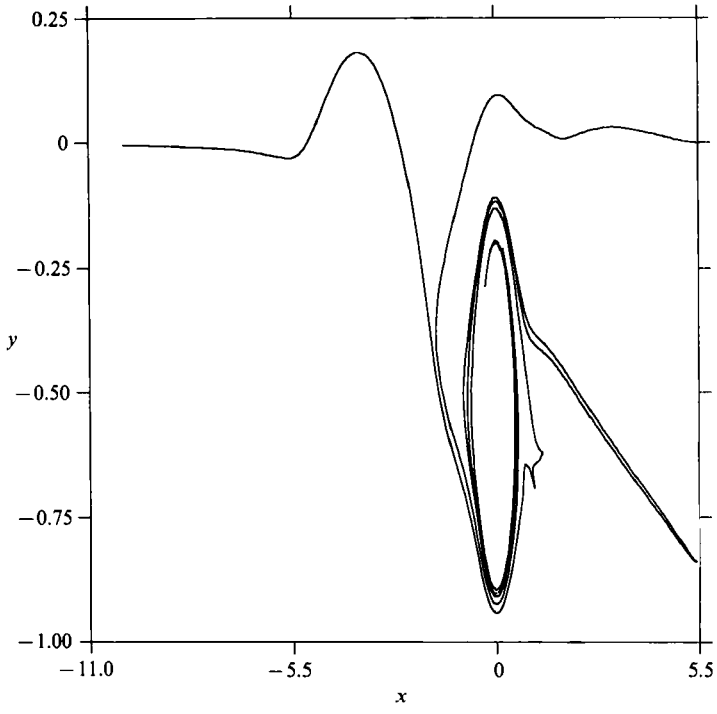

FIGURE 5. The $l = 1$ interface at $t = 12$ when a point vortex (unit circulation) replaces the round eddy. $R = -0.11$, $Q = -0.79$. The point vortex is located at $x = 0$, $y = -0.52$. The maximum in (4.1) occurs at $t = 8$.

Let s denote the arclength measured along $l = 1$ (figure 1*c*) from some fixed point far upstream on $l = 1$ to any other point, and let $H(s)$ denote the shortest (perpendicular) distance from the latter point to that branch of $l = 1$ which has wound counterclockwise around the eddy from the downstream side. Let $\epsilon \to 0$ denote a preassigned small distance (e.g. the Lagrangian point separation), and let $s_*(t)$ denote the smallest s for which $H(s) < \epsilon$ whenever such an s exists. Then the line segment $H(s_*)$ and the two $l = 1$ branches which it connects form a closed curve bounding an area $\alpha(\epsilon, t)$, part of which contains irrotational fluid, and the remainder $(\pi\rho^2)$ contains ζ_2 fluid. The existence of a limit for α (as $\epsilon \to 0$) is strongly suggested by the results for the $\zeta_2 = 3$, 2, 1.5 runs. But the final α is only approached asymptotically as time increases to infinity, and in order to define a mean entrainment rate we compute the time t at which

$$\text{Max}\,(\alpha(\epsilon, t)/t) \tag{4.1}$$

occurs, (this quantity also probably has an $\epsilon \to 0$ limit).

The procedure used to calculate (4.1) can be illustrated by referring to the $\zeta_2 = 1.5$ run at $t = 18$, when entrainment appeared to be near completion. At one of the interfacial points (s) we found $H = 0.085$ and $\alpha = 1.63$, and at a neighbouring s the values were $H = 0.033$, $\alpha = 1.61$. By adopting this $\epsilon = H = 0.033$ we found $\alpha = 1.65$ at $t = 20$, indicating that α increases slowly with t, and that the maximum in (4.1) occurs at $t = 18 \pm 1$. The values of $\alpha(t)$ obtained in this way for all the runs are listed in table 4.

In order to determine the relative importance of ζ_2 and ρ, similar (and simpler) contour dynamical calculations were also made for runs in which the round eddy was replaced by a point vortex (as in Stern & Flierl 1987) having the same circulation (namely unity). Figure 5 shows the evolution of the shear-layer interface when all the initial parameters (except ζ, ρ) are the same as in figure 2. Considering the arbitrariness and uncertainty in determining t (equation (4.1)), we conclude (table 4, rows 3 and 5) that α and t are roughly the same in the two cases, implying that the circulation $\hat{\Gamma}$ is more important than the individual values of $\hat{\zeta}_2$ and $\pi\hat{\rho}^2$. Table 4 also lists the results from other point-vortex calculations.

The total dimensional area $\alpha\hat{\lambda}^2$ entrained across the shear layer interface in the time $t\hat{\zeta}_1^{-1}$ can be set equal to an average velocity $\hat{V}_*$ acting across a distance equal to the scale length $\hat{\lambda}$, i.e. $\hat{V}_*(t\hat{\zeta}_1)\hat{\lambda} \equiv \alpha$, and this defines an 'entrainment velocity':

$$\hat{V}_* = \alpha/t(\hat{\Gamma}\hat{\zeta}_1)^{\frac{1}{2}}, \tag{4.2}$$

whose non-dimensional value (α/t) is also listed in table 4.

5. A jet of finite width

A real jet with finite half-width D will have vorticity disturbances on both sides, but we hypothesize that the interaction of the eddy with the nearest half of the jet is most important. Some support for this will be supplied by using a rigid boundary condition

$$v(x, -D, t) = 0 \tag{5.1}$$

at the nominal jet axis. This is formally equivalent to considering a symmetric jet (piecewise-uniform vorticity), and the 'symmetrical entrainment' of equal and opposite (point) vortices placed at equal distances from an axis at $y = -D$. This artifice eliminates the linear instability mechanism, and merely requires the introduction of image vortices into the previous contour dynamical equations. Note that these images ensure rapidly decreasing (x^{-2}) far-field velocities under all conditions, thereby allowing a greater range of initial conditions to be considered with greater confidence. The program for this case was tested by comparing its results with a liner analytical theory (small $\hat{\Gamma}$) similar to the one for $D = \infty$ given in the Appendix.

The initial parameters in the run for $D = 1.13$ (table 4) have the same values as those in figure 5. Essentially equal non-dimensional entrainment velocities occur for these two runs, and approximate equality was also obtained for $D = 0.85$ (table 4). Thus we conclude that in our range of calculations $\hat{V}_*/(\hat{\Gamma}\hat{\zeta}_1)^{\frac{1}{2}}$ is not sensitive to the distance of the jet axis from its edge.

When R is increased from -0.11 to $+0.12$ while keeping $(R-Q)$ at the same value as in the previous run ($D = 0.85$), the time required to complete entrainment (the last row in table 4) is more than doubled, but the non-dimensional entrainment velocity is only 25% smaller.

Although the initial $L_1(x, 0) < 0$ used in all the preceding runs appears to be a reasonable representation of the initial state of a disturbed shear layer in close contact with an eddy, this initial condition is admittedly arbitrary and adjustable. It therefore seemed desirable to reduce the number of such adjustable parameters by setting $L_1(x, 0) = 0$. Figure 6 shows the result for $R = 0.28$ and $D = 0.6$.

A question of accuracy may arise concerning the closely spaced spiral windings or filaments (e.g. figure 6), and therefore some of the calculations were repeated using

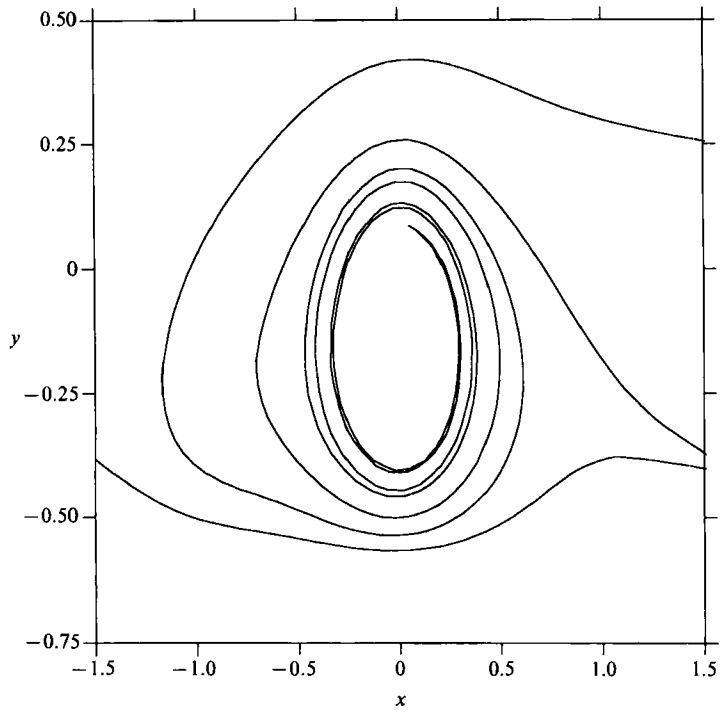

FIGURE 6. $L_1(x,0) = 0$ (i.e. $Q = 0$), $R = 0.28$, $D = 0.6$, and $t = 10$. Although the very thin filaments winding around the vortex are not precisely resolved, the error has a relatively negligible effect on the entrainment rate computed at $t = 9$. See text.

half the time step. The only noticeable difference was that the innermost filament on the left-hand side of the vortex (figure 6) was displaced one filament width to the right. Moreover, the calculations were continued, without computational instability, for a short time beyond the cutoff t (in (4.1)).

6. On the momentum flux of the mature entraining eddy

From two-dimensional kinematic consideration we know that the vorticity flux $v\zeta$ integrated between $x = \pm\infty$ equals the y-derivative of the horizontally integrated momentum flux $(-uv)$. When this relation is multiplied by y and then integrated we get

$$\int_{-\infty}^{+\infty}\int_{-D}^{\infty} \mathrm{d}x\,\mathrm{d}y\,vu = \iint yv\zeta\,\mathrm{d}\sigma, \tag{6.1}$$

where $\mathrm{d}\sigma = \mathrm{d}x\,\mathrm{d}y$. For the point-vortex model of the previous section there are two contributions to the last integral, one of which,

$$\iint y\zeta_2 v\,\mathrm{d}\sigma = \frac{1}{2}\frac{\mathrm{d}}{\mathrm{d}t}\bar{y}^2(t)\iint \zeta_2\,\mathrm{d}\sigma = \frac{1}{2}\frac{\mathrm{d}}{\mathrm{d}t}\bar{y}^2(t), \tag{6.2}$$

is due to the point vortex of unit circulation at $\bar{y}(t)$. The second contribution comes from the $\zeta = 1$ vortices inside a closed material curve consisting of $l = 1$, $y = -D$, and supplemented by two joining segments inserted at $x = \pm\infty$. (The latter move with

the local laminar velocity field $\bar{u}(y)$ at infinity.) The second contribution is obtained by letting $\mathrm{d}\sigma$ in (6.1) be a material area element, so that $\mathrm{d}/\mathrm{d}t(\mathrm{d}\sigma) = 0$. Since $v = \mathrm{d}y/\mathrm{d}t$ it then follows that the shear-layer contribution to (6.1) is

$$\iint yv\zeta_1 \,\mathrm{d}\sigma = \frac{1}{2}\frac{\mathrm{d}}{\mathrm{d}t}\iint y^2 \,\mathrm{d}\sigma = \frac{1}{6}\frac{\mathrm{d}}{\mathrm{d}t}\int_{-\infty}^{\infty} \mathrm{d}x[L_1^3(x,t) - (-D)^3] = \frac{1}{6}\frac{\mathrm{d}}{\mathrm{d}t}\int_{-\infty}^{\infty} L_1^3(x,t)\,\mathrm{d}x$$

and therefore

$$\iint \mathrm{d}x\,\mathrm{d}y\,vu = \frac{1}{2}\frac{\mathrm{d}}{\mathrm{d}t}[\bar{y}(t)]^2 + \frac{1}{6}\frac{\mathrm{d}}{\mathrm{d}t}\int_{-\infty}^{\infty} L_1^3(x,t)\,\mathrm{d}x. \tag{6.3}$$

For simplicity consider those runs in table 4 for which $L(x,0) = 0$). As the point vortex descends, $\bar{y}^2(t)$ decreases, the horizontal integral of L_1 remains at zero, but the horizontal integral of L_1^3 becomes negative. This is due to the predominance of those L_1 values underneath the descending vortex, as is apparent in figure 6, and as has been verified. Therefore integration of (6.3) from $t = 0$ to the entrainment time yields

$$\int \mathrm{d}t \int_{-\infty}^{+\infty}\int_{-D}^{\infty} \mathrm{d}x\,\mathrm{d}y\,vu < 0,$$

which implies that the entraining vortex transfers momentum up the mean gradient of $\bar{u}$.

Of course, a larger down-gradient momentum flux might have been produced in the process by which the eddy was generated (prior to $t = 0$ and the entrainment phase). Both of these flux types might occur at different times in the following modification of the classical Kelvin–Helmholtz problem. Consider a laminar and semi-infinite lower layer ($\zeta = 1$) separated from a semi-infinite irrotational upper layer by a thin intermediate layer of vorticity $\zeta = 2$. Inflexional instability will also occur in this non-symmetrical Kelvin–Helmholtz problem, and we expect that the finite-amplitude evolution will also lead to the mid-layer vorticity accumulating into 'cores'. During this eddy growth stage down-gradient momentum flux must occur, but it ceases as the eddy cores become fully developed. At this latter state we expect that the finite-amplitude evolution will interact with the $\zeta = 1$ vorticity of the semi-infinite lower layer in much the same way as in figure 1, i.e. the eddy cores will descend further into the $\zeta = 1$ shear layer, accompanied by a (small) up-gradient momentum flux, until the entrainment phase ends. This model seems to be simpler and more fundamental than the one considered here, but we have chosen to leave open the mechanism by which the mature eddy is generated.

7. Conclusion

A strong interaction of the outer edge of a jet with an eddy occurs when its maximum circulation $\hat{\Gamma}$ divided by its area is larger than the shear layer vorticity $\hat{\zeta}_1$, and when the initial distance $\hat{R}$ of the eddy from the edge is somewhat smaller than $\hat{\lambda} = (\hat{\Gamma}/\hat{\zeta}_1)^{\frac{1}{2}}$. The entrainment of the eddy and its surrounding irrotational fluid (figure 2) culminates in the formation of an essentially multi-connected ($l = 1$) interface. The 'pinching-off' process results in the formation of a 'new' edge of the shear layer, across which there has been a mean entrainment velocity (table 4)

$$\hat{V}_* = (0.11 \pm 0.02)\,(\hat{\Gamma}\hat{\zeta}_1)^{\frac{1}{2}}. \tag{7.1}$$

This accounts for all of the ($\zeta \neq 1$) fluid that has been incorporated (figure 2*e*) inside

the $\zeta = 1$ fluid, starting from an assumed initial state. The parametric range considered in obtaining (7.1) although far from complete, is believed to be relevant to the effect produced at the edge of a turbulent jet by a strong eddy, the latter having been generated upstream and earlier. The range includes neither extremely large values of $\hat{\zeta}_2/\hat{\zeta}_1$, for which the shear flow is dynamically passive, nor small values ($\leqslant 1$), for which the eddy is not entrained.

Wygnanski & Fiedler (1969) measured non-dimensional entrainment velocities $\bar{V}/U_0 = 0.03$ in a turbulent planar jet, where $\bar{V}$ is the local time-average transverse velocity near the edge of the irrotational region, and U_0 is the mean axial velocity at the same downstream position. In order to express $\bar{V}$ in terms of $(\hat{\Gamma}\hat{\zeta}_1)^{\frac{1}{3}}$ we must use the following crude similarity theory. If $\hat{D}$ is the local half-width of the jet, then $\hat{\zeta}_1 \sim U_0/\hat{D}$ is the order of magnitude of the vorticity near the jet's edge, $\hat{D}$ is the radius of a large-scale local eddy, and $\hat{\Gamma} \sim \hat{D}^2\hat{\zeta}_1$ is its circulation. Therefore $(\hat{\Gamma}\hat{\zeta}_1)^{\frac{1}{2}} \sim \hat{D}\hat{\zeta}_1 \sim U_0$, and $\bar{V} \sim 0.03(\hat{\Gamma}\hat{\zeta}_1)^{\frac{1}{3}}$ is the (crude) renormalization of the experimental data into our units. Since (7.1) is significantly larger than this $\bar{V}$, and since stochastic effects like intermittency have not been included, we conclude that the two-dimensional model is capable of accounting for the much more complicated effect in a turbulent flow.

The entrainment in figures 2–4 could also be regarded as the merger of a small eddy, having large vorticity, with a large (infinite-radius) eddy having smaller vorticity and vanishing velocity at its outer edge. The notable difference, compared to the classical problem of the merger of equal vortices, is that a large amount of ambient ($\zeta = 0$) fluid is incorporated into the big eddy along with the small one.

A countergradient momentum flux (6.3), produced by non-locally generated eddies, may be especially significant in oceanic jets where the energy flux as well as the mass flux increases downstream. But the model must obviously be generalized to include the baroclinic effects in this case.

I would like to acknowledge partial support of this work by the Office of Naval Research, and to thank Mr J. Bidlot (FSU) for his independent calculation of the spatially periodic cases mentioned in the text and the Appendix.

Appendix. Checking the numerical results for $D = \infty$

Consider first the problem (Stern 1985) of the free propagation of infinitesimal disturbances $[L(x,t)]$ on the $l = 1$ interface when the $l = 2$ eddy is absent. An elementary calculation shows that an $\bar{L}(k,t)\exp(-ikx)$ disturbance of wavenumber $k > 0$ propagates downstream with a frequency equal to half the reciprocal vorticity under $l = 1$, i.e. the linear wave equation is

$$\partial\bar{L}/\partial t = \tfrac{1}{2}i\bar{L}(k,t). \tag{A 1}$$

Let us solve the evolution problem for

$$L(x,t) \equiv \mathrm{Re}\int_0^\infty \bar{L}(k,t)\,\mathrm{e}^{-ikx}\,\mathrm{d}k,$$

when the initial value is such that

$$\bar{L}(k,0) = \mathrm{e}^{-ka} - \mathrm{e}^{-kb},$$

in which case $\bar{L}(0,0) = 0$. Thus the area bounded by $L(x,0)$ in $-\infty < x < \infty$

vanishes, and the net vorticity anomaly also vanishes. The same is true for the time-dependent solution

$$L(x,t) = \mathrm{Re}\, e^{it/2} \int_0^\infty dk\, e^{ikx} (e^{-ka} - e^{-kb}) = \mathrm{Re}\, e^{it/2} \left(\frac{a - ix}{a^2 + x^2} - \frac{b - ix}{b^2 + x^2} \right).$$

Note that in the limit when $b \to \infty$, with $a = O(1)$ and $x = O(1)$, the last term is negligible, so that the near-field solution is

$$L(x,t) = \mathrm{Re}\, e^{it/2} \frac{(a - ix)}{a^2 + x^2}$$

and this curve bounds an area (S_1) which varies with time. The far-field solution (the one involving b) is only necessary to account for global mass conservation. This example illustrates why S_1 is not conserved in the weak-interaction calculation (table 3), wherein the far-field velocity gives rise to interfacial ($l = 1$) disturbances which propagate (to $x = +\infty$) outside the truncated domain, producing uncompensated vorticity anomalies in the near field.

Next we modify this example by inserting an eddy of vorticity $\zeta_2 \to 0$ and unit radius (this is the lengthscale here), with the centroid at $x = 0$, $y = R = O(1)$, and we look for a linearized solution propagating steadily with speed $c \to 0$. To first order, the non-circular distortions of $l = 2$ may be neglected in computing the infinitesimal L_1. since $\partial L_1/\partial t$ and $u\,\partial L_1/\partial x$ are quadratically small, the velocity induced by the eddy on $y = 0$ (i.e. on $L_1(x) \to 0$) or

$$\frac{\zeta_2 x}{2(x^2 + R^2)} \equiv \tfrac{1}{2}\zeta_2 \,\mathrm{Re}\, i \int_0^\infty e^{-ikx} e^{-kR}\, dk$$

must be equal and opposite to the velocity $V_L(x)$ induced at the same point by the $L_1(x)$ vortex anomalies. The Fourier transform of this $V_L(x)$ is merely equal to the right-hand side of (A 1), and by equating velocities we get

$$V_L(x) = \tfrac{1}{2}\mathrm{Re} \int_0^\infty dk\, e^{-ikx}\, i\bar{L}(k) = -\tfrac{1}{2}\mathrm{Re} \int_0^\infty dk\, e^{-ikx}\, i\zeta_2 e^{-kR}.$$

Therefore $\bar{L}(k) = -\zeta_2 e^{-kR}$, and

$$L(x) = -\zeta_2 \,\mathrm{Re} \int_0^\infty dk\, e^{-ikx} e^{-Rk} = -\frac{\zeta_2 R}{x^2 + R^2}.$$

From this the small-vortex propagating speed

$$c = \zeta_2/4R$$

is easily computed by summing the horizontal velocities induced at $x = 0$, $r = R$ by all the vorticity anomalies bounded by L.

The result of this steady linear theory for $\zeta_2 = 0.01$ and $R = 1.5$ was compared with corresponding results ((2.3), (2.4a)) obtained from the numerical program (§3). Although the truncated domain $-10 < x < 10$ resulted in a 10% reduction of S_1 at $t = 0$, the initial values of c, u_1 (near $x = 0$) were all in very good agreement with the linear theory. For all x at $t = 8.25$ there was a departure of $v_1 \approx -1.2 \times 10^{-4}$ from the steady theoretical value (zero), and at $t = 12.5$ the value of c had decreased by 12%. When the length of the x-domain was doubled, the systematic v-error at $t = 8.5$ was reduced to -0.4×10^{-4}, and $\max|u_1|$ and $\max|L|$ deviated by only 3% from the

linear theory. At $t = 12.5$ the departure of c was reduced to 5% but part of this should be attributed to the analytic theory, since it neglects time-dependent effects appearing at small finite amplitude.

A further test of the nonlinear numerical calculation was obtained (as mentioned in the text) by comparing the $\zeta_2 = 1.5$ (table 3) calculation for an isolated eddy with one using a periodic array of eddies.

REFERENCES

CORCOS, J. M. 1981 The deterministic description of the coherent structure of free shear layers. In *The Role of Coherent Structures in Modelling Turbulence and Mixing* (ed. J. Jimenez). Lecture Notes in Physics, vol. **136**, pp. 10–40. Springer.

DRITSCHEL, D. G 1988 The repeated filamentation of two-dimensional vorticity interfaces. *J. Fluid Mech.* **194**, 511–517.

HUSSAIN, A. K. M. F. 1981 Coherent structures of perturbed and unperturbed jets. In *The Role of Coherent Structures in Modelling Turbulence and Mixing* (ed. J. Jimenez). Lecture Notes in Physics, vol. 136, pp. 252–291. Springer.

IKEDA, M. & LYGRE, K. 1989 Eddy-current interactions using a two layer quasi-geostrophic model. In *Mesoscale/Synoptic Coherent Structures in Geophysical Turbulence* (ed. J. C. J. Nihoul & B. M. Jamart), vol. 50, pp. 277–291. Elsevier.

MELANDER, M. V., OVERMAN, E. A. & ZABUSKY, N. J. 1986 Computational vortex dynamics in two and three dimensions. In *Proc. Workshop on Numerical Fluid Dynamics*. North-Holland.

POZRIKIDIS, C. & HIGDON, J. J. 1985 Nonlinear Kelvin Helmholtz instability of a finite vortex layer. *J. Fluid Mech.* **157**, 225–263.

PULLIN, D. I. 1981 The nonlinear behaviour of a constant vorticity layer at a wall. *J. Fluid Mech.* **108**, 401–421.

RICHARDSON, P. L. 1985 Average velocity and transport of the Gulf Stream near 55° W. *J. Mar. Res.* **73**, 83–111.

ROCKWELL, D. O. & NICCOLLS, W. O. 1972. Natural breakdown of planar jets, *Trans. ASME* D: *Basic Engng*, **94**, 720–730.

ROSHKO, A. 1981 The plane mixing layer. In *The Role of Coherent Structures in Modelling Turbulence and Mixing* (ed. J. Jimenez). Lecture Notes in Physics, vol. 136, pp. 208–217.

SMITH, D. C. & BIRD, A. A. 1989 Factors influencing asymmetry and self advection in ocean eddies. In *Mesoscale/Synoptic Coherent Structures in Geophysical Turbulence* (ed. J. C. J. Nihoul & B. M. Jamart), vol. 50, pp. 211–224. Elsevier.

STERN, M. E. 1985 Lateral wave breaking and shingle formation in shear flow. *J. Phys. Oceanogr.* **15**, 1274–1283.

STERN, M. E. & FLIERL, G. R. 1987 On the interaction of a vortex with a shear flow. *J. Geophys. Res.* **92**, (C10), 10733–10744.

STERN, M. E. & L. J. PRATT 1985 Dynamics of vorticity fronts. *J. Fluid Mech.* **161**, 513–532.

WYGNANSKI, I. & FIEDLER, H. 1969 Some measurements in the self preserving jet. *J. Fluid Mech.* **38**, 577–612.

ZABUSKY, N. J., HUGHES, M. H. & ROBERTS, K. V. 1979 Contour dynamics for the Euler equations in two dimensions. *J. Comput. Phys.* **30**, 96–106.